Fermilab FERMILAB-Conf-02/214-T Sept. 2002
nuhep-exp/02-012
UCD-02-11

New results for a photon-photon collider

David Asner,[1] Bohdan Grzadkowski,[2] John F. Gunion,[3] Heather E. Logan,[4]
Victoria Martin,[5] Michael Schmitt,[5] and Mayda M. Velasco[5]

[1] *Lawrence Livermore National Laboratory, Livermore, CA*
[2] *Institute of Theoretical Physics, Warsaw University, Warsaw, Poland*
[3] *University of California, Davis, California 95616, USA*
[4] *Theoretical Physics Department, Fermilab, PO Box 500, Batavia, Illinois 60510-0500, USA*
[5] *Northwestern University, Evanston, Illinois, USA*

(Dated: August 24, 2002)

We present new results from studies in progress on physics at a two-photon collider. We report on the sensitivity to top squark parameters of MSSM Higgs boson production in two-photon collisions; Higgs boson decay to two photons; radion production in models of warped extra dimensions; chargino pair production; sensitivity to the trilinear Higgs boson coupling; charged Higgs boson pair production; and we discuss the backgrounds produced by resolved photon-photon interactions.

I. INTRODUCTION

This document summarizes recent results obtained by the American working group on $\gamma\gamma$ colliders, and is intended to be a supporting document for discussions at LC2002, to be held on Jeju Island, South Korea.

We have been considering two machine scenarios. In the first, a 'Higgs-factory' is based on high energy photon beams optimized for the s-channel production of a Standard Model-like Higgs boson of mass in the range 100–130 GeV. The properties of this Higgs boson would be explored in a dedicated fashion. Paramount among these is the measurement of $\Gamma_{\gamma\gamma}$, which is sensitive to new charged particles such as the top squark, and also the top Yukawa coupling. Certain rare decays are available due to low backgrounds, such as $h \to \gamma\gamma$, $h \to \gamma Z$, and $h \to Z Z^*$. For an earlier study and description of the machine, see Ref. [1]. In the second, more conventional scenario, a $\gamma\gamma$ collider runs in parallel with a high energy e^+e^- linear collider. In this case the study of the heavier neutral Higgs bosons, H and A, can be pursued even in cases in which they are not visible in the companion e^+e^- machine [2]. Linearly polarized beams provide information about the charge-parity (CP) nature of these particles, so in this and in other senses a $\gamma\gamma$ collider complements the e^+e^- machine. As discussed in this document, effective cross sections are as large as or larger than the corresponding e^+e^- cross sections. For example, we have studied the copious and clean signal from $\gamma\gamma \to H^+H^-$. Also, it appears that the sensitivity of a high energy $\gamma\gamma$ collider to the Higgs self-coupling is about the same as the e^+e^- machine. A similar conclusion is reached for chargino production. While one would not advocate substituting a high energy e^+e^- collider by a $\gamma\gamma$ one, it is clear that more will be understood about the Higgs (and other) sector if both machines are in operation.

This paper is organized as follows. In Sec. II we describe how the mass of the heavier top squark can be inferred from a measurement of the $h^0\gamma\gamma$ coupling in the minimal supersymmetric Standard Model (MSSM), if the lighter top squark mass and mixing angle are known. In Sec. III we examine Higgs boson decay to two photons. In Sec. IV we examine radion production in two-photon collisions in models of warped extra dimensions. In Sec. V we study chargino pair production in two-photon collisions and estimate the event yield. In Sec. VI we study pair production of the Standard Model (SM) Higgs boson in two-photon collisions, which is sensitive to the trilinear Higgs boson coupling. In Sec. VII we study signal and background to charged Higgs boson pair production in two-photon collisions, with decays to taus. In Sec. VIII we examine the background at a two-photon collider due to resolved photons. Finally we summarize our results in Sec. IX.

II. TOP SQUARK PARAMETERS FROM MSSM HIGGS BOSON PRODUCTION IN PHOTON-PHOTON COLLISIONS

A two-photon collider optimized to run on a light Higgs boson (h^0) s-channel resonance can measure the rate of $\gamma\gamma \to h^0 \to b\bar{b}$ with a precision of about 2% [1–4]. Combining this with the expected model-independent measurement of BR($h^0 \to b\bar{b}$) of 2-3% from an e^+e^- collider [5, 6], one can extract the $h^0\gamma\gamma$ coupling with a precision of 2-3%. In the MSSM, such a measurement is sensitive to contributions to the loop-induced $h^0\gamma\gamma$ coupling from supersymmetric (SUSY) particles, mainly top squarks and charginos [7], and to deviations in the couplings of h^0 to SM particles from their SM values. We show that this measurement of the $h^0\gamma\gamma$ coupling can be combined with e^+e^- collider data on the lighter top squark mass and mixing angle to constrain the mass of the heavier top squark to within about ± 20 GeV or less, if the lighter top squark is not too heavy.

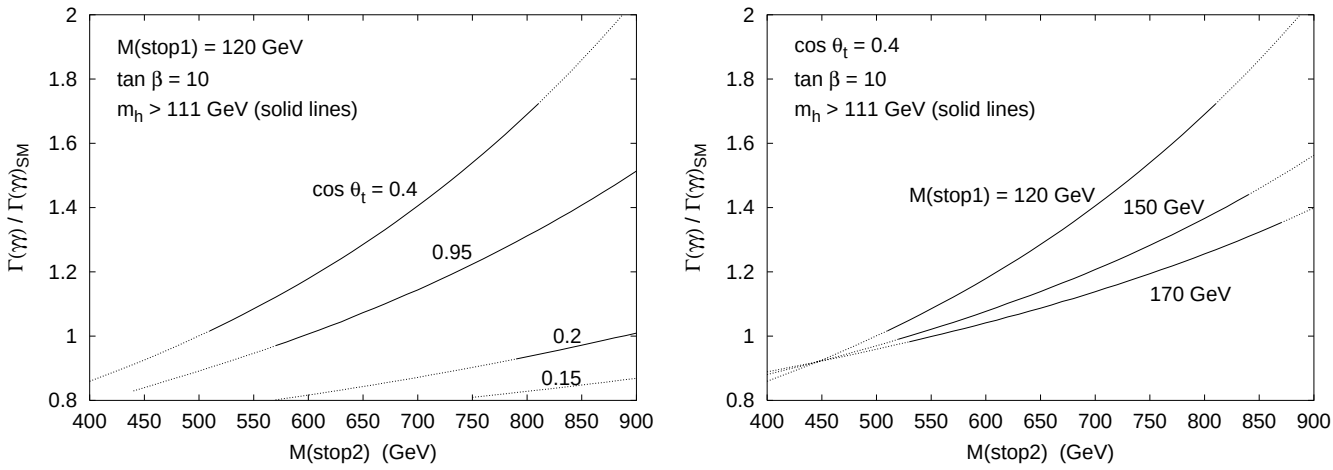

FIG. 1: Dependence of the partial width $\Gamma(h^0 \to \gamma\gamma)$ on $m_{\tilde{t}_2}$ for various values of $m_{\tilde{t}_1}$ and $\cos\theta_{\tilde{t}}$. Here $m_A = 1$ TeV, $\tan\beta = 10$, $M_2 = -\mu = 200$ GeV, and the remaining SUSY mass parameters are set to 1 TeV. The numerical calculations were done using HDECAY [10].

In the MSSM, there can generally be a large splitting between the masses of the lighter ($\tilde{t}_1$) and heavier ($\tilde{t}_2$) top squarks, and $\tilde{t}_1$ can be quite light. Thus, one can envision a situation in which $\tilde{t}_1$ can be pair-produced at a first-stage (500 GeV) e^+e^- collider, but $\tilde{t}_2$ is kinematically inaccessible. In this case, $m_{\tilde{t}_1}$ can be measured to high precision. The top squark mixing angle $\cos^2\theta_{\tilde{t}}$ can also be measured at the per cent level because of the dependence of the $e^+e^- \to \tilde{t}_1\tilde{t}_1^*$ cross section on this angle.

In such a situation one would like to constrain the mass of $\tilde{t}_2$ indirectly. In the decoupling limit of large m_A, the $h^0\tilde{t}_i\tilde{t}_j^*$ couplings can be written solely in terms of known SM parameters and $m_{\tilde{t}_1}$, $m_{\tilde{t}_2}$ and $\cos\theta_{\tilde{t}}$, with a very mild additional dependence on $\cos 2\beta$. A measurement of one of these couplings then allows one to extract $m_{\tilde{t}_2}$. The cross sections for $e^+e^- \to \tilde{t}_1\tilde{t}_1^*h^0$ [8] and $e^+e^- \to \tilde{t}_1\tilde{t}_1^*Z$ [9] are sensitive to the $h^0\tilde{t}_1\tilde{t}_1^*$ coupling and hence to $m_{\tilde{t}_2}$. This method succeeds only if $\tilde{t}_1$ is light enough and $\cos\theta_{\tilde{t}}$ is moderate (i.e., not close to 1 or 0). For $m_{\tilde{t}_1} = 120$ GeV and $\cos\theta_{\tilde{t}} = 0.4$, the sensitivity to $m_{\tilde{t}_2}$ is about ± 20 GeV from $e^+e^- \to \tilde{t}_1\tilde{t}_1^*h^0$ [8]. This method is no longer effective if the $h^0\tilde{t}_1\tilde{t}_1^*$ coupling is small, since the cross section becomes too small to detect.

Here we study the sensitivity to $m_{\tilde{t}_2}$ of the $h^0 \to \gamma\gamma$ partial width, assuming that $m_{\tilde{t}_1}$ and $\cos\theta_{\tilde{t}}$ have been measured in e^+e^- collisions. This is shown in Fig. 1 for various values of $m_{\tilde{t}_1}$ and $\cos\theta_{\tilde{t}}$, in the large-m_A limit. Using the knowledge of $m_{\tilde{t}_1}$ and $\cos\theta_{\tilde{t}}$ from the e^+e^- collider, a 2% measurement of $\Gamma(h^0 \to \gamma\gamma)$ allows one to extract $m_{\tilde{t}_2}$ with a statistical precision of about ± 10 GeV for $m_{\tilde{t}_1} = 120$ GeV and $\cos\theta_{\tilde{t}} = 0.4$. This precision worsens as $m_{\tilde{t}_1}$ increases or $\cos\theta_{\tilde{t}}$ varies, because the dependence of $\Gamma(h^0 \to \gamma\gamma)$ on $m_{\tilde{t}_2}$ becomes weaker (see Fig. 1). The soft SUSY-breaking mass parameters M_{Q_3}, M_{U_3} and $X_t \equiv A_t - \mu\cot\beta$ can then be inferred from $m_{\tilde{t}_1}$, $\cos\theta_{\tilde{t}}$ and $m_{\tilde{t}_2}$.

Additional uncertainties arise due to the dependence on m_A of the $h^0\tilde{t}_i\tilde{t}_j^*$ couplings and additional chargino loop contributions to $\Gamma(h^0 \to \gamma\gamma)$. To a lesser extent, the bottom squarks also contribute at large $\tan\beta$ [11]. In most of the MSSM parameter space, values of m_A below about 600 GeV will lead to at least a 2σ deviation in the ratio $\mathrm{BR}(h^0 \to b\bar{b})/\mathrm{BR}(h^0 \to WW)$, measurable in either e^+e^- [6, 12] or $\gamma\gamma$ [4] collisions. For larger m_A, the effect on $\Gamma(h^0 \to \gamma\gamma)$ is negligible. Values of m_A as low as 200 GeV lead to an additional ± 4 GeV parametric uncertainty in $m_{\tilde{t}_2}$ for the parameters considered above.

The uncertainty due to chargino loops can be removed if the parameters of the chargino mass matrix are already known. The measurements are straightforward at an e^+e^- collider [13]. In fact, complete reconstruction of the chargino and neutralino mass matrices is possible even if only $\tilde{\chi}_1^+$, $\tilde{\chi}_1^0$ and $\tilde{\chi}_2^0$ are kinematically accessible [14]. If $\tilde{\chi}_1^+$ is too heavy to be pair produced in 500 GeV e^+e^- collisions, its effect on $\Gamma(h^0 \to \gamma\gamma)$ is also diminished due to decoupling. For $M_2 = -\mu = 250$ GeV (leading to a $\tilde{\chi}_1^+$ mass of 200-214 GeV, depending on $\tan\beta$), the unknown chargino contribution leads to an additional ± 8 GeV uncertainty in $m_{\tilde{t}_2}$ for the parameters considered above, assuming no knowledge of the value of $\tan\beta$. If $\tan\beta$ is large, the chargino contribution is quite small and leads to far less uncertainty.

Finally, we comment briefly on Higgs boson decays. Decays of h^0 into $b\bar{b}$, WW, ZZ, $\gamma\gamma$ and $Z\gamma$ can be measured at a two-photon collider. The theoretical behavior of these decay widths in the MSSM has been analyzed thoroughly [7, 12, 15]. Neglecting contributions of SUSY particles in the loop, the ratio $\Gamma(h^0 \to Z\gamma)/\Gamma(h^0 \to WW)$ approaches its SM value very quickly with increasing m_A; the deviation from the SM prediction is less than 10% for $m_A > 130$

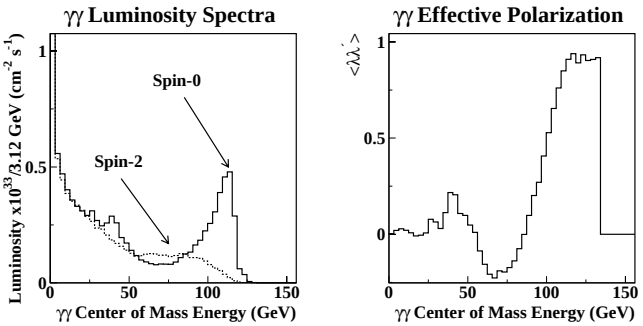

FIG. 2: Luminosity for a 10^7 sec year and associated expectation value for the product of photon polarizations, $\langle\lambda\lambda'\rangle$, are plotted for $\sqrt{s}_{ee} = 150$ GeV ($x = 4.1$ for 1.054/3 μm laser wavelength), assuming 80% electron beam polarizations.

GeV and less than 2% for $m_A > 150$ GeV. Thus a measurement of this ratio can be used as a test for light charged non-SM particles in the $h^0 \to Z\gamma$ loop. Ref. [15] found that top squarks can contribute up to 5% deviations for $m_{\tilde{t}_1} > 100$ GeV and charginos can contribute up to 10% deviations for $m_{\tilde{\chi}_1^+} > 100$ GeV.

III. HIGGS BOSON DECAY TO TWO PHOTONS

The partial width for $h \to \gamma\gamma$, $\Gamma_{\gamma\gamma}$, is sensitive to charged non-SM particles. For example, in the MSSM with a light and a heavy stop, the mass of the heavier stop can be inferred from the measured value of $\Gamma_{\gamma\gamma}$ if the mass of the lighter stop and the mixing angle are already known – see Section II. Since the Higgs cross section is proportional to $\Gamma_{\gamma\gamma}$, the rate $\gamma\gamma \to b\bar{b}$ when combined with a measurement of $BR(h \to b\bar{b})$ from an e^+e^- collider leads to a 2–3% measurement of $\Gamma_{\gamma\gamma}$ [1, 4].

The channel $h \to \gamma\gamma$ is doubly sensitive to $\Gamma_{\gamma\gamma}$. In an e^+e^- experiment, this channel can be difficult to observe due to large backgrounds. But in a $\gamma\gamma$ collider, the backgrounds are low because continuum scattering $\gamma\gamma \to \gamma\gamma$ proceeds only through loops. Preliminary studies have shown that a clear signal can be extracted with a very simple analysis, provided the calorimeter performance is good enough. Furthermore, a direct measurement of the Higgs mass is possible from the $\gamma\gamma$ invariant mass distribution. We have continued these studies and made them more realistic, as briefly described here; the conclusions remain positive.

This study assumes a Higgs-factory machine, running with the peak of the $\gamma\gamma$ energy spectrum at the Higgs mass. For $m_h = 120$ GeV, this corresponds to 75 GeV electron beams [1]. The beam parameters for this facility are given in Table I and the corresponding luminosity and polarization spectra in Fig. 2. The assumed integrated luminosity is sufficient to produce 11,400 Higgs bosons. The SM branching ratio for $m_h = 120$ GeV is 2.1×10^{-3}.

The first improvement is the introduction of a calorimeter geometry and simulation. An aggressive design has been assumed, with coverage down to 3° and a high degree of granularity. The energy resolution is the same as the CMS design, namely, $\sigma_E/E = \left((0.015/\sqrt{E})^2 + (0.0045)^2\right)^{1/2}$. A cone algorithm is used to find the high energy photon showers. Threshold and clustering effects have little impact on the mass resolution, but do lead to a shift in the observed mass of 0.25 GeV. The width of the cone, $\Delta R = 0.3$, was chosen as small as possible without impacting the signal resolution.

Next we introduced resolved photon backgrounds – see Section VIII for details. Events simulated with Pythia are overlayed with the signal and background events before clustering. Significant 'extra' energy occasionally lands within the cluster cone, leading to a reconstructed mass that is higher than the true mass. It also partially compensates for the loss due to threshold and clustering effects. The reconstructed mass distribution has a tail to high values, as shown in Fig. 3.

The parametrization of the $\gamma\gamma \to \gamma\gamma$ background was handled as before. However, a new background was considered, in which Compton scattering gives an energetic electron and photon in the detector with the electron mis-identified as a photon. This happens if the tracking device or track reconstruction fail, or if the electron radiates most of its energy while passing through the beam pipe or Silicon vertex detector. As a starting point, we took the electron mis-identification to be $\epsilon_{e\to\gamma} = 10^{-4}$. This gives a background roughly as large as the background from $\gamma\gamma \to \gamma\gamma$. Such a small value for $\epsilon_{e\to\gamma}$ may require a special detector design.

The distribution of reconstructed $\gamma\gamma$ mass is shown in Fig 3. Besides the smooth distribution from $\gamma\gamma \to \gamma\gamma$, which ends at $M_{\gamma\gamma} = 130$ GeV, the contribution from Compton scattering is shown, extending up to $M_{\gamma\gamma} = 135$ GeV. The

Electron Beam Energy (GeV)	75	250
β_x/β_y (mm)	2/0.020	4/0.065
ϵ_x/ϵ_y ($\times 10^{-8}$)	140/5	360/7.1
σ_x/σ_y (nm)	138/2.6	172/3.1
σ_z (microns)	30	156
N ($\times 10^{10}$)	0.4	1.5
e^- Polarization (%)	80	80
repetition rate (Hz)	$100 \times 154 \times 11$	120×95
Laser Pulse Energy (J)	1.0/70%=1.4	1.0
Laser λ (microns)	$1.054/3 = 0.351$	1.054
CP-IP distance (mm)	1	2

TABLE I: Laser and electron beam parameters for $\sqrt{s}_{ee} = 150$ GeV and $\sqrt{s}_{ee} = 500$ GeV. The beam parameters for $\sqrt{s}_{ee} = 500$ GeV differ from the NLC-e^+e^- parameters. The bunch charge has been doubled to improve luminosity. Consequently both the vertical emittance, ϵ_y, and the bunch length, σ_z are increased. Additionally, the total current is conserved as the repetition rate reduced by a factor of 2. The optimal laser wavelength decreases as the beam energy decreases. We assume that non-linear optics are used to triple the laser frequency for the $\sqrt{s}_{ee} = 150$ GeV machine and that this procedure is 70% efficient, thus more laser power is required.

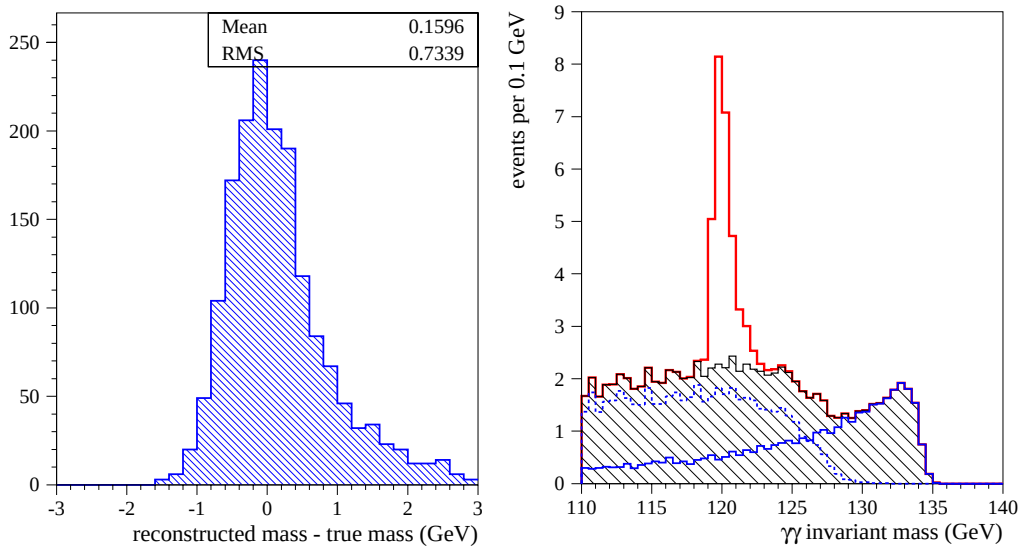

FIG. 3: (left) The reconstructed Higgs mass compared to the true mass. (right) The mass distribution, including backgrounds from $\gamma\gamma \to \gamma\gamma$ (dashed line extending to ~ 130 GeV) and $e\gamma \to e\gamma$ (heavy solid line extending to ~ 135 GeV) as well as the signal (peak at 120 GeV). The hatched histogram shows the sum of background contributions.

difference in shape can be exploited to discriminate the two contributions. The signal peak is clearly visible, despite the smearing due to the resolved photon background.

IV. THE ROLE OF PHOTON-PHOTON COLLISIONS IN EXPLORING THE SCALAR SECTOR OF THE RANDALL-SUNDRUM MODEL.

The scalar sector of the Randall-Sundrum (RS) model comprises the Higgs boson and the radion. In general, the bare radion and bare Higgs boson mix by virtue of a $\xi R H^\dagger H$ mixing contribution to the visible brane Lagrangian. A non-zero value for ξ is certainly allowed by all symmetries, and so large values of $|\xi|$ are a possibility. The phenomenology of the Higgs boson, h, and radion, ϕ, mass eigenstates is strongly dependent upon ξ. To fully explore and test the scalar sector phenomenology of the h and ϕ will require a full complement of accelerators. Here, we briefly sketch the crucial role of a $\gamma\gamma$ collider in verifying the scalar sector structure. This work uses the procedures

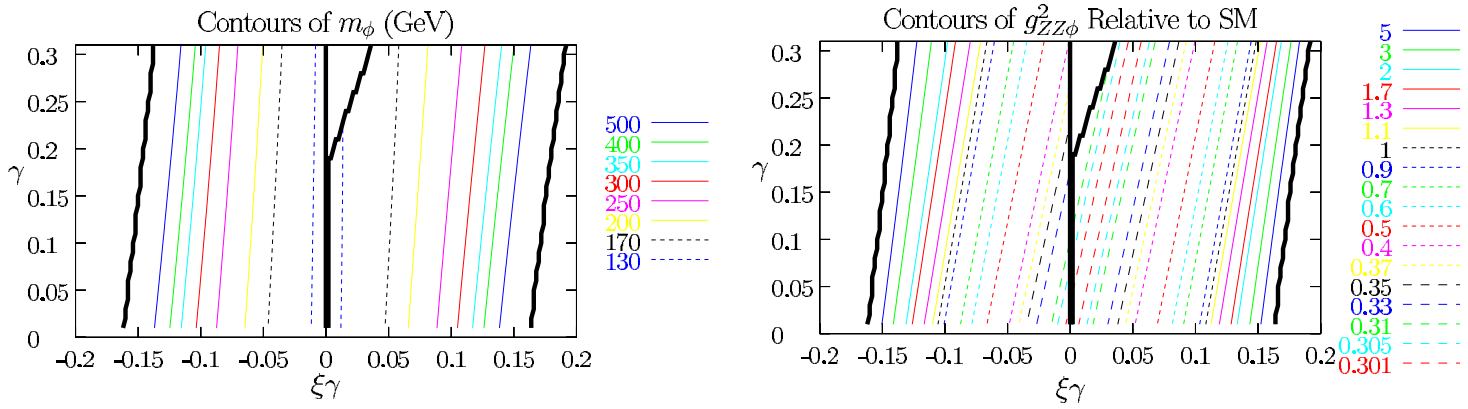

FIG. 4: Contours of m_ϕ and $g^2_{fV\phi}$ in the $(\xi\gamma, \gamma)$ parameter space for fixed $m_h = 120$ GeV and $g^2_{fVh} = 0.7$. Solid black contours indicate the boundaries imposed by theoretical consistency and LEP/LEP2 direct discovery limits. Where the inner two black boundaries at $\xi\gamma \simeq 0$ are next to one another, there is no actual boundary. For simplicity, in this plot we have not displayed a 2nd set of solutions to $m_h = 120$ GeV, $g^2_{fVh} = 0.7$ that emerge for small $|\xi\gamma|$ values.

of Ref. [16] for analyzing the RS scalar sector.

The basic structure of the scalar sector is fixed by the four parameters, m_h, m_ϕ, ξ and $\gamma \equiv v/\Lambda_\phi$ where $v = 246$ GeV and Λ_ϕ is the vacuum expectation value of the bare radion field, a new physics scale that should lie roughly in the range 1 TeV to 20 TeV, resulting in a range for γ from 0.25 down to 0.01 (we will consider values as high as 0.31). A very important constraint on the parameter space is provided by requiring that the kinetic energy terms of the diagonalized Lagrangian not be tachyonic. Algebraically, this reduces to the requirement that $Z^2 \equiv 1 + 6\xi\gamma^2(1-6\xi) > 0$. This constraint implies a maximum value of $|\xi|$ of order $1/\gamma$. A second crucial constraint on the m_h, m_ϕ, ξ, γ parameter space comes from the requirement that inversion to the bare parameters $m^2_{h_0}$ and $m^2_{\phi_0}$ be possible. This requirement implies that the minimum value of $|m_\phi - m_h|$ must increase with increasing $|\xi|$, with $m_\phi = m_h$ only possible for zero mixing, $\xi = 0$.

For our discussion, it will be convenient to replace m_ϕ by another observable, namely g^2_{ZZh} which will be very well determined in $e^+e^- \to Zh$ production at a future e^+e^- linear collider (LC), independently of any information regarding the ϕ. The interesting question is then whether the $\gamma\gamma$ collider can play an important role given other possible measurements of h and ϕ production at the Large Hadron Collider (LHC) and the LC.

Let us write $h_0 = dh + c\phi$ and $\phi_0 = a\phi + bh$, where a, b, c, d are functions of the four parameters used to specify the scalar sector. All $f\overline{f}$ and VV ($V = W, Z$) couplings of the physical h [ϕ] are given by $g_{fVh} = (d + \gamma b)$ [$g_{fV\phi} = (c + \gamma a)$] times the value for a SM Higgs boson. The sum rule, $g^2_{fVh} + g^2_{fV\phi} = R^2$, where $R^2 = \left[1 + \frac{\gamma^2(1-6\xi)^2}{Z^2}\right]$, will play an important role below; R^2 is clearly ≥ 1 (and possibly substantially larger than 1 given that small values of Z^2 are possible). The gg and $\gamma\gamma$ couplings of the h and ϕ receive anomalous contributions from their ϕ_0 components proportional to γb and γa as well as from SM particle loops proportional to g_{fVh} and $g_{fV\phi}$, respectively. These anomalous couplings are very crucial to unraveling the RS scalar sector and it is the ability of a $\gamma\gamma$ collider to probe the anomalous $\gamma\gamma$ coupling that would be of particular value.

We illustrate the general strategy by focusing on just one possible case. We imagine that the linear collider (and LHC) find a Higgs boson of mass $m_h = 120$ GeV and that the LC determines $g^2_{fVh} = 0.7$ (from the measurement of g^2_{ZZh}) with very small error bars ($\lesssim 3-5\%$ should be achievable, see [17]). The sum rule noted above implies that $g^2_{fV\phi} \geq 0.3$ (possibly substantially so) and, therefore, if the ϕ is not too heavy, the ϕ too will be observable in $e^+e^- \to Z\phi$ production at the LC and possibly also observable at the LHC. In such a case, m_ϕ and $g^2_{fV\phi}$ will be well measured. Assuming that the RS scenario is correct and that these measurements both have very high experimental precision, this will be sufficient to determine the location in m_h, m_ϕ, ξ, γ space up to a two-fold ambiguity. This is illustrated in Fig. 4.[1] One need only locate the two points (one in the $\xi < 0$ region and one in the $\xi > 0$ region) at which the contours for the measured value of $g^2_{fV\phi}$ crosses those for the measured value of m_ϕ. Of course, if $g^2_{fV\phi}$ is measured with less than perfect precision, additional ambiguity in the parameter space location will result. It is also

[1] For the case being considered it is unlikely that the ϕ is too heavy to be observed since a heavy ϕ would probably be inconsistent with precision electroweak constraints for $g^2_{fV\phi} \geq 0.3$.

important to note from Fig. 4 that $m_\phi > m_h$ (as is generally the case if $g^2_{fVh} < 1$) with values of m_ϕ close to m_h only allowed when $|\xi\gamma|$ is relatively small. However, the contours with $m_\phi > 300$ GeV displayed are problematical. Given the associated $g^2_{fV\phi}$ values, the radion contributions to precision electroweak observables might be in conflict with current constraints.

There is still one further ambiguity. Namely, given just the measurements mentioned so far, it would not be possible to say for certain which of the two particles detected should be identified with the eigenstate h most closely connected to the bare Higgs field and which should be identified with the ϕ that derives from the radion.

Given the inevitable errors for the $g^2_{fV\phi}$ and g^2_{fVh} measurements,[2] the above-mentioned two-fold ambiguity, and the possible misidentification of h vs. ϕ, it will be crucial to have additional measurements to fully determine the parameter space location. In this regard, we must first repeat the important fact that all $f\overline{f}$ and VV couplings depend only on the combinations g_{fVh} and $g_{fV\phi}$. Further, the h total width is only mildly sensitive to γb, with the consequence that its $f\overline{f}$ and VV branching ratios are only weakly dependent upon γb. Thus, all rates involving only $f\overline{f}$ and/or VV initial and final states are almost entirely determined by the value of g^2_{fVh}, which we have assumed to be well-measured with a value of 0.7. For the case being considered where $g^2_{fV\phi}$ is possibly as big or bigger than g^2_{fVh}, similar statements apply to the ϕ. In particular, once $m_\phi > 2m_W$, the WW and ZZ branching ratios of the ϕ are substantial and rather insensitive to γa. (Total widths measured directly or indirectly would also not provide a clear identification of ϕ vs. h in the case considered.)

To clarify these ambiguities, it will be vital to measure h and ϕ production/decay channels involving gg and/or $\gamma\gamma$ that are sensitive to the gg and/or $\gamma\gamma$ anomalous couplings. There are four very useful possibilities. By performing all four measurements it will also be possible to fully test the structure of the RS theory, including the anomalous gg and $\gamma\gamma$ couplings of the h and ϕ. The four process are $gg \to h \to \gamma\gamma$, $\gamma\gamma \to h \to b\overline{b}$, $gg \to \phi \to X$ ($X = \gamma\gamma$ for $m_\phi \lesssim 150$ GeV or $X = W^+W^-, ZZ$ for $m_\phi \gtrsim 150$ GeV) and $\gamma\gamma \to \phi \to X'$ ($X' = b\overline{b}$ for $m_\phi \lesssim 160$ GeV and $X' = W^+W^-, ZZ$ for $m_\phi \gtrsim 160$ GeV.) The ratios of these rates to the corresponding rate for a SM Higgs boson of the same mass are shown in Fig. 5. In exploring the implications of these plots, one needs to keep in mind that the $\gamma\gamma \to \phi \to b\overline{b}$ rates are only substantial for $m_\phi \lesssim 140$ GeV, where measurements at the $\sim 3\%$ level are possible in the case of the SM Higgs [2]. For higher m_ϕ, the $\gamma\gamma \to \phi \to W^+W^-, ZZ$ rates are generally robust but experimental studies of the accuracy with which they can be measured are not available.

We note that there is a certain complementarity between the $gg \to \phi$ rates and the $\gamma\gamma \to \phi$ rates. In particular, where the $gg \to \phi \to \gamma\gamma$ and ZZ rates are too suppressed to be detectable ($0 < \gamma\xi < 0.15$, $\gamma \div 0.05 - 0.1$), the $\gamma\gamma \to \phi \to b\overline{b}$ and ZZ rates remain adequate for reasonably precise measurement.

Fig. 5 shows that the $\gamma\gamma \to h \to b\overline{b}$ rate is only very modestly sensitive to parameter space location, whereas the $\gamma\gamma \to \phi \to b\overline{b}$ and $\gamma\gamma \to \phi \to ZZ$ rates are very sensitive to the choice of $(\xi\gamma, \gamma)$. The h eigenstate would then be identified as that consistent with the predicted rate for one of the two possible choices for parameters consistent with the observed $m_h, m_\phi, g^2_{fVh}, g^2_{fV\phi}$ values. The $gg \to h \to \gamma\gamma$ rate would then provide an extremely good determination of the precise location in $(\xi\gamma, \gamma)$ parameter space (given the roughly 'orthogonal' nature of the rate contours as compared to m_ϕ and $g^2_{fV\phi}$ contours). The corresponding ϕ rates would also serve this purpose while at the same time verifying the typically much larger anomalous $\gamma\gamma$ and gg couplings of the ϕ (determined by γa which is much bigger than γb over most of parameter space).

Indeed, if we look at the $\gamma\gamma \to \phi \to b\overline{b}$ contours at small $|\xi\gamma|$ where $m_\phi \lesssim 140$ GeV (see Fig. 4), so that $BR(\phi \to b\overline{b})$ is substantial, we see in Fig. 5 dramatic and for the most part accurately measurable (where the rate is a substantial fraction of the SM rate) variation of the rate as a function of γ, allowing an accurate determination of γ that can be checked against the determination from h measurements. If we look along the $m_\phi = 300$ GeV contours of Fig. 4, $BR(\phi \to ZZ)$ will be big and Fig. 5 shows strong variation of the $gg \to \phi \to ZZ$ and $\gamma\gamma \to \phi \to ZZ$ rates, which rates should be accurately measurable where suppression relative to the SM is not large. Note that all these rates are very different for $\xi\gamma < 0$ as compared to $\xi\gamma > 0$ and will strongly distinguish between the $\xi\gamma < 0$ and $\xi\gamma > 0$ contour crossings in Fig. 4 that give the same m_ϕ and $g^2_{fV\phi}$ values.

In fact, by using all these measurements, a model independent determination of the anomalous couplings of the h and ϕ is possible. We define

$$R_{sgg} \equiv \frac{g^2_{sgg}(\text{with anomaly})}{g^2_{sgg}(\text{without anomaly})}\,, \quad \text{and} \quad R_{s\gamma\gamma} \equiv \frac{g^2_{s\gamma\gamma}(\text{with anomaly})}{g^2_{s\gamma\gamma}(\text{without anomaly})}\,, \tag{1}$$

for $s = h$ and $s = \phi$. The procedure for determining R_{sgg} and $R_{s\gamma\gamma}$ in a model-independent manner is the following.

---

[2] The masses m_h and m_ϕ will be extremely well measured and errors in these quantities will not be an issue.

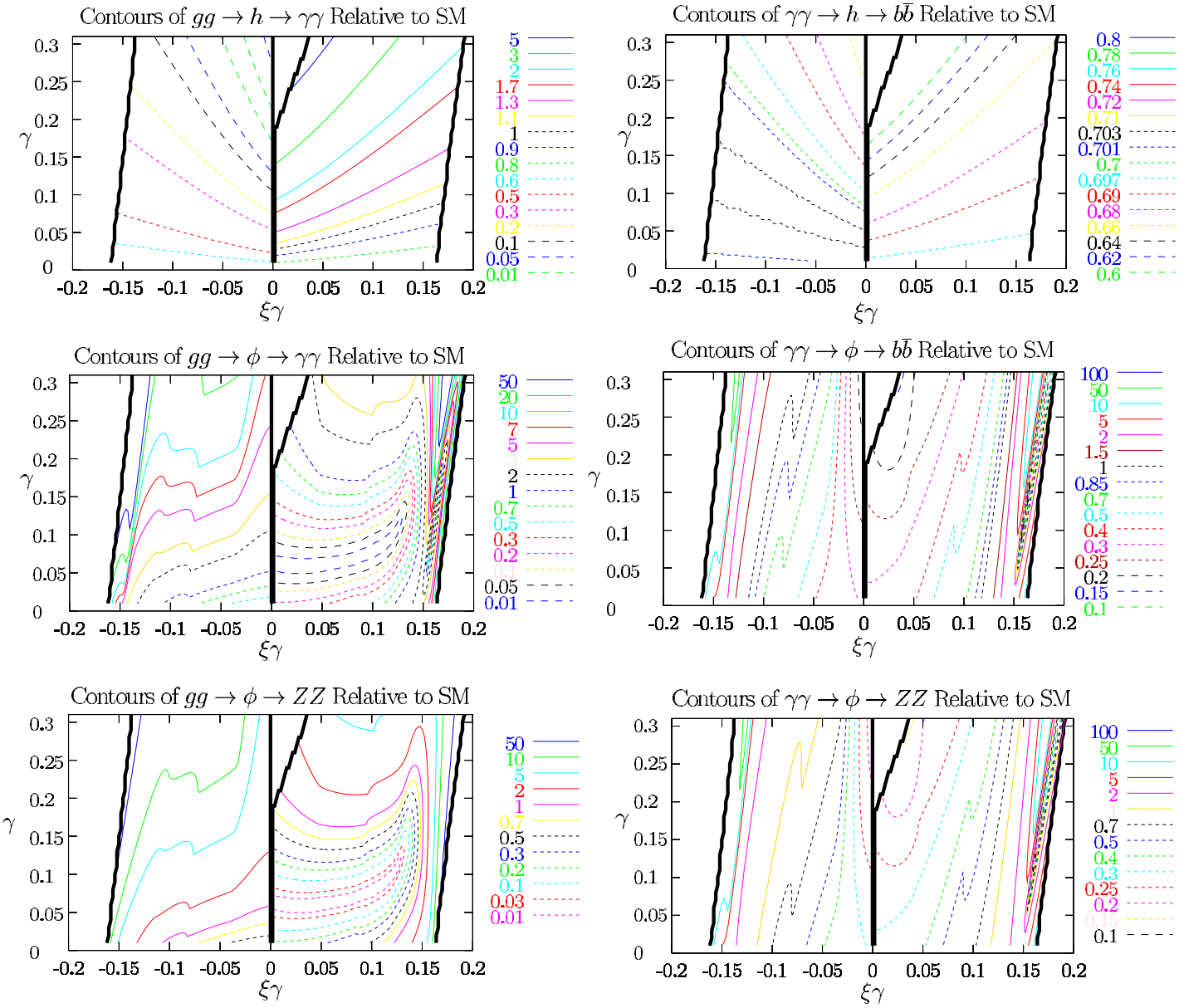

FIG. 5: Contours of rates (relative to a SM Higgs of the same mass) for $gg \to h \to \gamma\gamma$, $gg \to \phi \to \gamma\gamma$, $gg \to \phi \to ZZ$. $\gamma\gamma \to h \to b\bar{b}$, $\gamma\gamma \to \phi \to b\bar{b}$, and $\gamma\gamma \to \phi \to ZZ$ in the $(\xi\gamma, \gamma)$ parameter space for fixed $m_h = 120$ GeV and $g^2_{fVh} = 0.7$. Solid black contours indicate the boundaries imposed by theoretical consistency and LEP/LEP2 direct discovery limits. Where the inner two black boundaries at $\xi\gamma \simeq 0$ are next to one another, there is no actual boundary. For simplicity, in this plot we have not displayed a 2nd set of solutions to $m_h = 120$ GeV, $g^2_{fVh} = 0.7$ that emerge for small $|\xi\gamma|$ values. Note that contours of a given ratio value for $\gamma\gamma \to \phi \to b\bar{b}$ and $\gamma\gamma \to \phi \to ZZ$ coincide according to the RS model.

(We assume for purposes of illustration that the ϕ is light enough that its branching ratio to W^+W^-, ZZ final states is small.)

First, obtain g^2_{ZZs} (defined relative to the SM prediction at $m_{h_{SM}} = m_s$) from $\sigma(e^+e^- \to Zs)$ (inclusive recoil technique). Next, determine $BR(s \to b\bar{b}) = \sigma(e^+e^- \to Zs \to Zb\bar{b})/\sigma(e^+e^- \to Zs)$. Then, $g^2_{s\gamma\gamma}$(from experiment) $= \sigma(\gamma\gamma \to s \to b\bar{b})/BR(s \to b\bar{b})$ (note the need for the $\gamma\gamma$ collider measurement). One would then compute

$$R_{s\gamma\gamma} \equiv \frac{g^2_{s\gamma\gamma}(\text{from experiment})}{g^2_{h_{SM}\gamma\gamma}(\text{as computed for } m_{h_{SM}} = m_s) \times g^2_{ZZs}(\text{from experiment})} \tag{2}$$

To determine g^2_{sgg} experimentally requires one more step. We must compute $\sigma(gg \to s \to \gamma\gamma)/BR(s \to \gamma\gamma)$. To

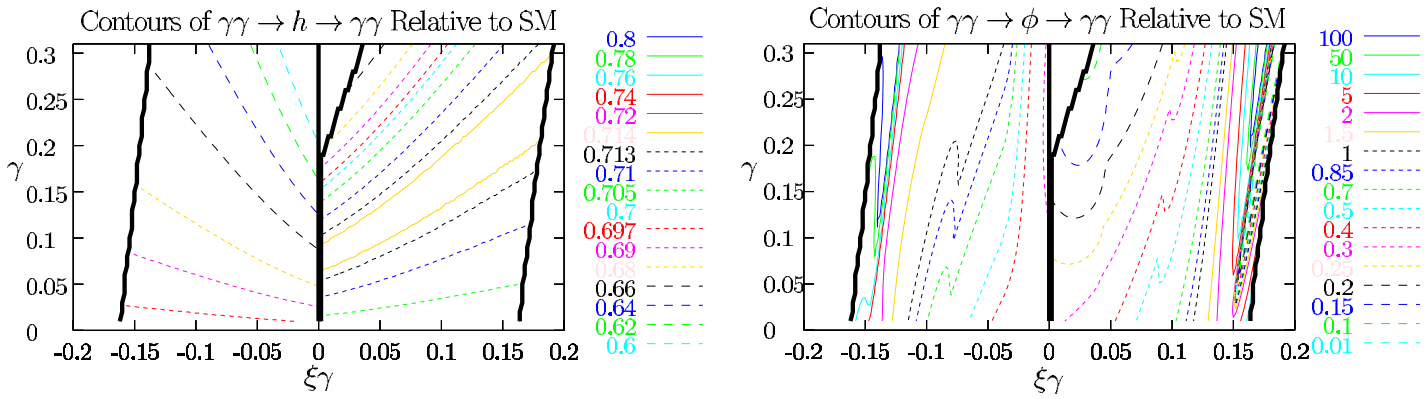

FIG. 6: Contours of rates (relative to a SM Higgs of the same mass) for $\gamma\gamma \to h \to \gamma\gamma$ and $\gamma\gamma \to \phi \to \gamma\gamma$ in the $(\xi\gamma, \gamma)$ parameter space for fixed $m_h = 120$ GeV and $g^2_{fVh} = 0.7$, with conditions and conventions as in Fig. 5.

obtain $BR(s \to \gamma\gamma)$, we need a measurement of $\Gamma^{\rm tot}_s$. Given such a measurement, we then compute

$$BR(s \to \gamma\gamma) = \frac{\Gamma(s \to \gamma\gamma)(\text{computed from the experimentally determined } g^2_{s\gamma\gamma})}{\Gamma^{\rm tot}_s(\text{from experiment})}\,, \tag{3}$$

where the above experimental determination of $g^2_{s\gamma\gamma}$ is employed and the experimental techniques outlined in [17] are employed for $\Gamma^{\rm tot}_s$. The ratio analogous to Eq. (2) for the gg coupling is then

$$R_{sgg} \equiv \frac{g^2_{sgg}(\text{from experiment})}{g^2_{h_{SM}gg}(\text{as computed for } m_{h_{SM}} = m_s) \times g^2_{ZZs}(\text{from experiment})}\,. \tag{4}$$

For a light SM Higgs boson, the various cross sections and branching ratios needed for the $s\gamma\gamma$ coupling can be determined with errors of order a few percent. A careful study is needed to assess the errors in the case of the h and ϕ of the RS scalar sector.

Finally, it is interesting to see what roles the $\gamma\gamma \to h \to \gamma\gamma$ and $\gamma\gamma \to \phi \to \gamma\gamma$ rate measurements might play. (We see from the previous section that determination of the $\gamma\gamma \to h_{SM} \to \gamma\gamma$ rate would be possible with $\sim 10\%$ accuracy after a few years of operation for $m_{h_{SM}} \sim 120$ GeV.) We plot contours of these rates (relative to the corresponding h_{SM} rate) in Fig. 6. As expected, with $g^2_{fVh} = 0.7$ fixed, the $\gamma\gamma \to h \to \gamma\gamma$ rate is roughly 0.7 times the SM value, but with up to $\sim 15\%$ variation in either direction depending upon location in $(\xi\gamma, \gamma)$ parameter space. Thus, measurement of this rate with the expected accuracy would be an interesting check and constraint on the RS model. The $\gamma\gamma \to \phi \to \gamma\gamma$ rate shows a lot of variation in the small $|\xi\gamma|$ region where $m_\phi \lesssim 140$ GeV (see Fig. 4), *i.e.* for m_ϕ such that $BR(\phi \to \gamma\gamma)$ would be large enough that the rate might be measurable. However, for many such parameter points, the suppression relative to the SM comparison rate is sufficiently substantial that the accuracy of the measurment would be relatively poor. Still, if other aspects of the RS model are verified, this would be a very interesting final check on the model. In particular, the ratio of the $\gamma\gamma \to \phi \to \gamma\gamma$ rate relative to the SM comparison differs substantially from the corresponding ratios for $\gamma\gamma \to \phi \to b\overline{b}$ and ZZ (as plotted in Fig. 5) at any given $(\xi\gamma, \gamma)$ parameter location.

V. CHARGINO PAIR PRODUCTION IN PHOTON-PHOTON COLLISIONS

We study the potential for determining the chargino masses and mixing angles in two-photon collisions at a future linear collider. These parameters determine the fundamental SUSY parameters: M_2, μ, $\tan\beta$, and the CP-violating phase $\cos\Phi_\mu$.

At an e^+e^- collider, the chargino pair production cross sections are sensitive to the mixing angles via the chargino couplings to the Z boson. Thus, by combining mass and cross section measurements from e^+e^-, one can extract the fundamental parameters of the chargino sector [13]. The situation is complicated, however, by the fact that the chargino production cross section in e^+e^- collisions receives radiative corrections of up to 10% that depend on additional SUSY parameters [18].

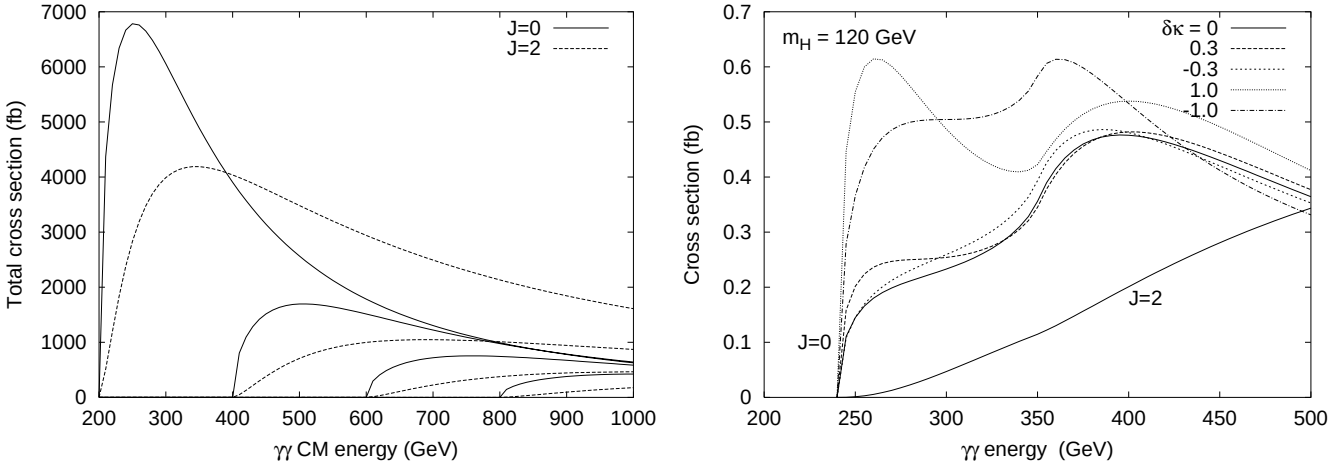

FIG. 7: (left) Parton-level cross sections in fb for chargino pair production in two-photon collisions as a function of the two-photon center-of-mass energy, for total photon helicity $J = 0$ (solid curves) and 2 (dashed curves). (right) Parton-level cross section for $\gamma\gamma \to HH$ as a function of the $\gamma\gamma$ center-of-mass energy, for $J = 0$ and $J = 2$. Shown also are the effects of varying the trilinear coupling.

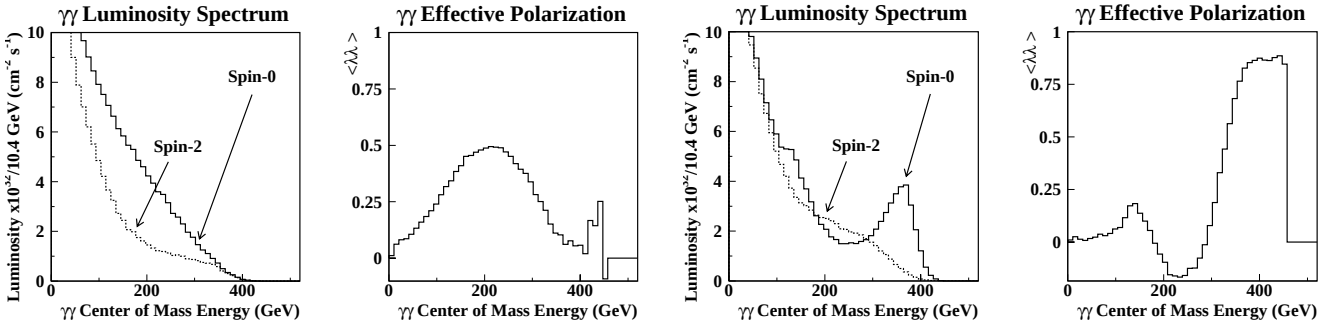

FIG. 8: Luminosity, in units $fb^{-1}/10.4$ GeV, for a 10^7 sec year and associated expectation value for the product of photon polarizations, $\langle\lambda\lambda'\rangle$, are plotted for $\sqrt{s}_{ee} = 500$ GeV ($x = 4.5$ for 1.054 μm laser wavelength), assuming 80% electron beam polarizations, for polarization orientation cases type-I (left) and type-II (right).

At a $\gamma\gamma$ collider, unfortunately, there is no sensitivity to the chargino mixing angles in the tree-level production, because the photon-chargino couplings depend only on the electric charge. [3] However, chargino pair production at a photon collider can still be used to measure the chargino mass. In addition, the parameter independence of the production cross section allows one to study the chargino decay dynamics in a theoretically clean way and offers sensitivity, e.g., to M_1 and the sneutrino mass through the branching ratio and forward-backward asymmetry in the decay $\tilde{\chi}_1^+ \to \tilde{\chi}_1^0 e^+ \nu_e$ [19]. Beyond the tree level, radiative corrections due to quark and squark loops can modify the cross section in $\gamma\gamma$ collisions by up to 3% [20]. Of course, radiative corrections to the chargino masses [21] are relevant in either collider environment. Fig. 7 shows the polarized parton-level chargino production cross sections [22].

Our study incorporates a "Pantaleo" final focus [23] optimized for $\gamma\gamma$ collisions [24] and realistic two-photon spectra based on the most probable available laser technology [25]. We use the laser and electron beam parameters given in Table I and the CAIN [26] Monte Carlo program to obtain the luminosity and polarization spectra plotted in Fig. 8. The CAIN simulation of the interaction between the laser photons and the primary electron beam, and the Compton scattered photons and the spent electron beam, includes the effects due to beamstrahlung, secondary collisions and other non-linear effects. These effects provide large corrections to the naive luminosity distributions first considered in Ref. [27, 28]. The $J = 0$ cross section turns on quickly, since it goes like β at threshold, while the $J = 2$ cross section goes like β^3. In e^+e^-, the cross section goes like β at threshold.

[3] The decay of charginos provides some sensitivity to the mixing angles.

	$\int \mathcal{L}_{th}$ (fb^{-1}/10^7 s)	σ (fb)	Event yield
Spin-0	30	3000	90,000
Spin-2	5	1000	5,000
e^+e^-	160	300	48,000

TABLE II: Comparison of the integrated luminosity above threshold ($\int \mathcal{L}_{th}$), the "average" cross section (σ), and the event yield per Snowmass year of 10^7 sec for pair production of charginos of mass 150 GeV in $\gamma\gamma$ and e^+e^- collisions.

	$\sqrt{s_{ee}} = 500$ GeV			$\sqrt{s_{ee}} = 800$ GeV		
	$\int \mathcal{L}_{th}$ (fb^{-1}/10^7 s)	σ (fb)	Event yield	$\int \mathcal{L}_{th}$ (fb^{-1}/10^7 s)	σ (fb)	Event yield
Spin-0	40	0.3	13	120	0.3	39
Spin-2	20	0.1	1-2	60	0.2	1-2
e^+e^-	160	0.2	32	250	0.15	38

TABLE III: Comparison of the integrated luminosity above threshold ($\int \mathcal{L}_{th}$), the "average" cross section (σ), and the event yield per Snowmass year of 10^7 sec for double-Higgs production in $\gamma\gamma$ and e^+e^- collisions. We assume $m_h = 120$ GeV.

The estimated event yield is given in Table II, assuming a chargino mass of $m_{\tilde{\chi}_1^+} = 150$ GeV, along with the cross section and luminosity described above. The chargino yield is a factor of two greater in two-photon collisions than in e^+e^-. Because the final state is the same, we expect the signal reconstruction efficiency to be similar to that in e^+e^-. Thus, it may possible to determine the chargino masses more precisely in $\gamma\gamma$ collisions. Further study is required since the $\gamma\gamma$ luminosity spectrum, shown in Fig. 2 and Fig. 8, does not have a sharp end point. Luminosity beyond the naive kinematic limit is due to multiple Compton interactions. A sharper end point can be obtained by reducing the laser power and thus the probability for multiple Compton interactions however the total luminosity is also reduced. The optimal laser power for end point mass measurements has not been determined.

This is a report on a work in progress. Future reports will include full background and detector simulation.

VI. MEASURING THE TRILINEAR COUPLING OF THE STANDARD MODEL HIGGS BOSON

We examine the potential for determining the trilinear coupling of the Standard Model Higgs boson in two-photon collisions at a future linear collider. The trilinear Higgs boson coupling can be measured in e^+e^- collisions [29, 30]. There is also some sensitivity to the trilinear Higgs coupling at the LHC [31]. This is a direct test of the shape of the Higgs potential. Accuracies of approximately 20% on the $e^+e^- \to ZHH$ cross section can be obtained for M_H in the range of 120 GeV to 140 GeV with 1000 fb^{-1} at $\sqrt{s}_{ee} = 500$ GeV. A neural network improves the sensitivity to 13% for M_H=120 GeV. The sensitivity is diluted to 22% by additional amplitudes which are insensitive to the trilinear coupling.

We use the cross sections for SM Higgs boson pair production in polarized two-photon collisions computed in Ref. [32]. The trilinear Higgs boson coupling enters the diagram containing a virtual s-channel Higgs boson, which contributes only to the $J = 0$ amplitude. To evaluate the sensitivity of the cross section to the trilinear Higgs coupling, we introduce an anomalous trilinear Higgs coupling in a gauge-invariant way, following Ref. [32]:

$$\delta\mathcal{L}_{\rm Higgs} = -\frac{\delta\kappa}{2}\frac{m_H^2}{v}\left[H^3 + \frac{3}{v}G^+G^-H^2\right] + \cdots, \tag{5}$$

where $v = 246$ GeV is the Higgs vacuum expectation value, H is the SM Higgs field, $G^\pm$ are the charged Goldstone bosons, and $\delta\kappa$ is the dimensionless anomalous trilinear Higgs coupling normalized so that for $\delta\kappa = 1$, the anomalous term will cancel the SM H^3 coupling. We computed the one-loop integrals with the help of the LoopTools package [33]. Fig. 7 shows the parton-level cross sections for $\gamma\gamma \to HH$ for $J = 0$ and $J = 2$, for the SM (solid lines) and including an anomalous trilinear coupling (dashed lines).

To estimate the event yields, given in Table III, in an NLC-like machine, we use the machine assumptions described in Sec. V. The spin-0 event yield is about 3 times as large at $\sqrt{s_{ee}} = 800$ GeV. since more of the twp-photon luminosity spectrum is above HH threshold.

We estimate that production rates for $e^+e^- \to HHZ$ and $\gamma\gamma \to HH$ at an 800 GeV linear collider are comparable. In e^+e^- collisions, the reconstruction efficiency of the ZHH final state is 43% [30]. We expect it to be better

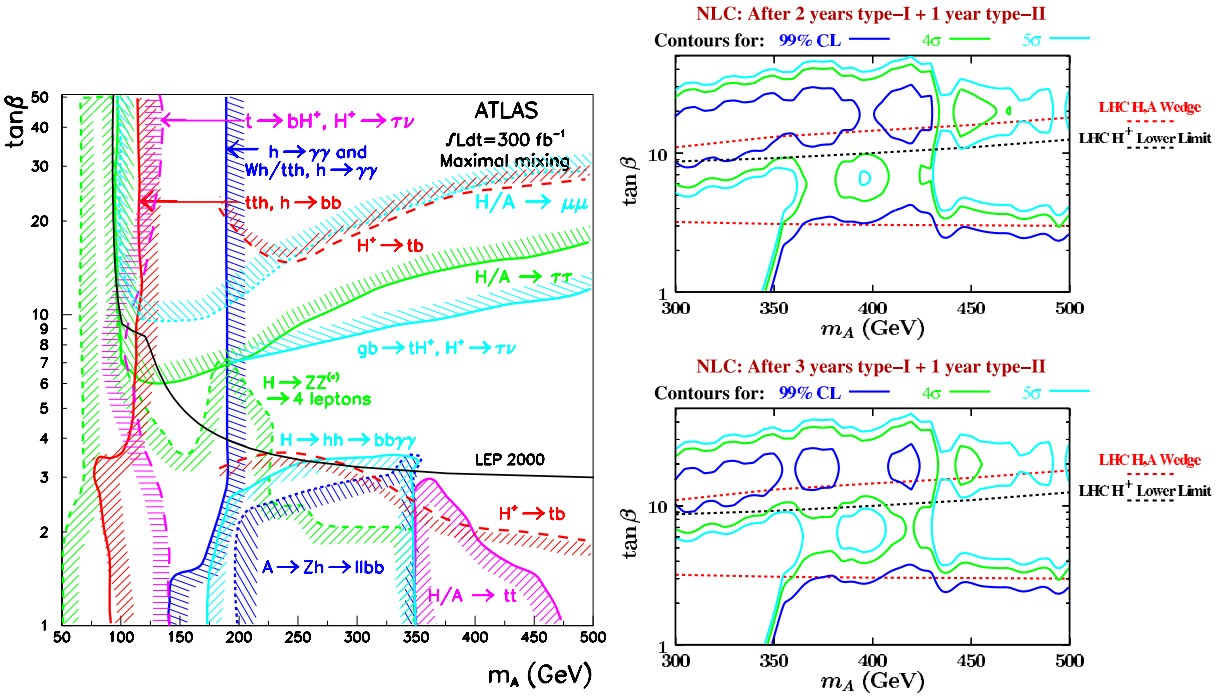

FIG. 9: (left) 5σ discovery contours for MSSM Higgs boson detection in various channels are shown in the $[m_{A^0}, \tan\beta]$ parameter plane, assuming maximal mixing and an integrated luminosity of $L = 300$ fb^{-1} for the ATLAS detector. This figure is preliminary [34]. Note that $\gamma\gamma \to H^+H^-$is a potential discovery mode for $\gamma\gamma$ as the $H^\pm$ will be undetected at the LHC for $m_{H^\pm} > 125$ GeV and moderate $\tan\beta$. (right) The dashed lines delineate the LHC wedge region. The 4σ and 5σ discovery contours for H^0, A^0 in the $\gamma\gamma \to H^0, A^0 \to b\bar{b}$ channel are shown. For the case where the H^0, A^0 are unobserved, the 99% exclusion contour is shown. In just 3 years of operation at design luminosity the H^0, A^0 would be discovered (excluded) in about 2/3 (nearly all) of the LHC wedge region [2].

than this in $\gamma\gamma$ collisions, because of the simpler HH final state. The dominant background in both analyses is $e^+e^-/\gamma\gamma \to WW$. We estimate comparable sensitivity to the cross section per running time in $\gamma\gamma$ or e^+e^- collisions at $\sqrt{s}_{ee} = 800$ GeV. As in e^+e^- collisions, the sensitivity to the trilinear coupling my be diluted due to additional amplitudes contributing to $\gamma\gamma \to HH$.

This is a report on a work in progress. Future reports will include full background and detector simulation.

VII. PROSPECTS FOR OBSERVING CHARGED HIGGS BOSONS IN GAMMA-GAMMA COLLISIONS

In the case of the two-doublet MSSM Higgs sector there are five physical Higgs bosons - two CP-even, h^0 and H^0 (with $m_{h^0} < m_{H^0}$), one CP-odd, A^0, and a charged Higgs pair, $H^\pm$. The ability to detect $\gamma\gamma \to H^0, A^0, H^+H^-$ will be of greatest importance if the heavy Higgs bosons cannot be detected either at the LHC or in e^+e^- collisions at the LC. In fact, there is a significant section of parameter space in the MSSM, often referred to as the LHC 'wedge' region, for which this is the case.

We have studied the prospects for $\gamma\gamma \to H^0, A^0$ [2] where we conclude that a $\gamma\gamma$ collider can provide Higgs signals for the H^0 and A^0 over a possibly crucial portion of parameter space in which the LHC and direct e^+e^- collisions at a LC will not be able to detect these Higgs bosons or their $H^\pm$ partners. This is illustrated in Fig. 9. In this section we discuss the prospects for observing charged Higgs bosons from the interaction $\gamma\gamma \to H^+H^-$. This is a potential discovery mode for $\gamma\gamma$ as the $H^\pm$ will be undetected at the LHC for $m_{H^\pm} > 125$ GeV and moderate $\tan\beta$.

This study assumes a e^-e^- machine with $\sqrt{s_{ee}} = 500$ GeV and 80% electron polarization. The CAIN Monte Carlo program [26] is used to model the luminosity spectra for two configurations of laser polarization, type-I and type-II, described in Section V. The luminosity spectra are shown in Fig. 8. In both of these configurations one Snowmass year of 10^7 sec running would correspond to a total integrated luminosity of 4×10^{32} cm^{-2}s^{-1} or 400 fb^{-1}.

A mass range for $H^\pm$ from the lower experimental bound of $m_{H^\pm} \approx 80$ GeV/c^2 up to the kinematic limit of $m_{H^\pm} = 200$ GeV/c^2 is considered. For $m_{H^\pm} < m_t$ the main decay mode is $H^+ \to \tau^+\nu_\tau$ as the decay modes to Wh^0 and $t\bar{b}$ are suppressed.

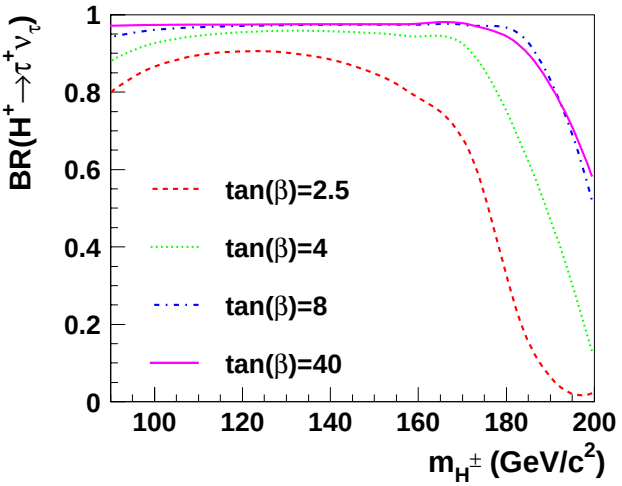

FIG. 10: MSSM predictions of the branching ratio for the process $H^+ \to \tau^+\nu_\tau$ as a function of $m_{H^\pm}$, for various $\tan\beta$ values.

Fig. 10 shows the MSSM prediction for the branching ratio of $H^+ \to \tau^+\nu_\tau$ as a function of $m_{H^\pm}$. The values were obtained by running the HDECAY program [10]. A value of 500 GeV/c^2 was used for the SUSY breaking mass parameters. For most values of $\tan\beta$ the branching ratio is between 80% and 98% when $m_{H^\pm} < m_t$. To allow these results to be interpreted independently of the branching ratio, the number of events over branching ratio squared are presented. Pandora-Pythia [35] was used to calculate effective cross section for $\gamma\gamma \to H^+H^-$, taking into account the luminosity spectra. The results for the two beam types is shown in Fig. 12.

Backgrounds to the $\gamma\gamma \to H^+H^-$ process come from both τ and W-pair production. The cross section for $\gamma\gamma \to \tau^+\tau^-$ is around 300 pb and for $\gamma\gamma \to W^+W^- \to \tau^+\tau^-$ is approximately 220 fb for the type-II beam. For a charged Higgs mass of 140 GeV/c^2 these backgrounds are factors of approximately 5,000 and 4 times the signal cross section.

Three empirically reconstructable variables were used to study the signal and background processes: the cosine of the angle of the tau-jet in the detector, $\cos(\theta)$, the sum of transverse momenta of all the visible particles from the tau decays, $\Sigma p_T(\tau)$, and the acoplanarity of the two tau jets, $Acop = \cos^{-1}(\vec{p}_{T1} \cdot \vec{p}_{T2}/(p_{T1}p_{T2}))$. We reject background with the requirements that $|\cos(\theta)| < 0.8$, $Acop < 3$ and $\Sigma p_T(\tau)/\mathrm{GeV}c^{-1} > 35 + 25 \cdot (Acop - \frac{\pi}{2})^2$. Fig. 11 shows these three quantities for the signal and two background processes

These requirements reduce the $\gamma\gamma \to \tau^+\tau^-$ background by a factor of more than 10^{-6}, therefore this background can be ignored. The acceptance of the W-pair production background is around 0.5%, while keeping around 10% of the signal for $m_{H^\pm} = 140$ GeV/c^2.

Fig. 12 shows the number of events expected per Snowmass year, divided by the $H^+ \to \tau^+\nu_\tau$ branching ratio squared. The dashed horizontal line the plots indicates the the number of $\gamma\gamma \to W^+W^-$ events.

It can be seen the type-II beam configuration is the best for observing $\gamma\gamma \to H^+H^-$. At a charged Higgs mass of 140 GeV/c^2, around 1250 events/BR$(H^+ \to \tau^+\nu_\tau)^2$ would be observed per Snowmass year, to be compared with about 300 $\gamma\gamma \to W^+W^- \to \tau^+\tau^-$ events.

For $\tan\beta \gtrsim 4$ the signal to background ratio is greater than 1 for $m_{H^\pm} \lesssim m_t$. For smaller values of $\tan\beta$ the signal to background is better than 1 up to charged Higgs masses of about 160 GeV/c^2. The type-I beam would also be useful for observing $\gamma\gamma \to H^+H^-$ for $m_{H^\pm} \lesssim 130$ GeV/c^2.

It is not possible to reconstruct a mass-type variable for the $\gamma\gamma \to H^+H^-$ events, as there are too many unknown kinematic quantities. Studies using detector simulation are under way to look for observables correlated with $m_{H^\pm}$.

In conclusion, for moderate values of $\tan\beta$ it will be possible to observe $\gamma\gamma \to H^+H^-$ events using a 500 GeV e^-e^- collider for all masses up to the top quark mass. This will probe some of the MSSM parameter space where the $H^\pm$ will be undetected at the LHC ($m_{H^\pm} > 125$ GeV and moderate $\tan\beta$). The process $\gamma\gamma \to H^+H^- \to t\bar{t}b\bar{b}$ will probe the remaining region of parameter space in which the $H^\pm$ would be undetected at the LHC.

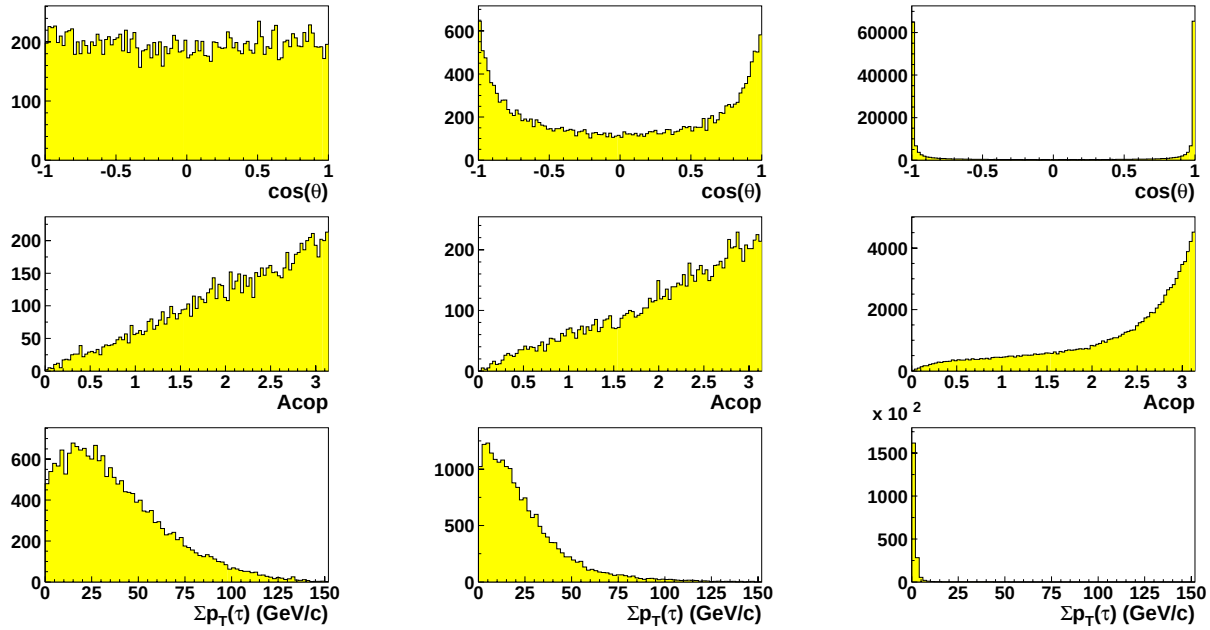

FIG. 11: The three observable quantities defined in the text. The left plots are for H^+H^- events, the center plots are for W-pair production and the right plots are for τ-pair production.

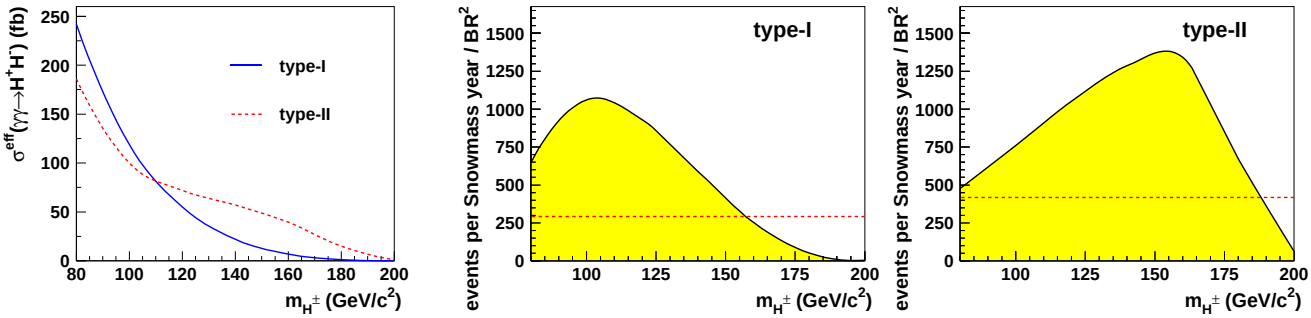

FIG. 12: On the left: The effective cross section for $\gamma\gamma \to H^+H^-$ for the two beam configurations. The center and right plots show the number of accepted events per BR$(H^+ \to \tau^+\nu_\tau)^2$ per Snowmass year, as a function of $m_{H^\pm}$. The dashed horizontal line shows the number of accepted background $\gamma\gamma \to W^+W^-$ events.

VIII. RESOLVED PHOTON BACKGROUNDS

The photon is the gauge boson of QED. The photon couples, via virtual charged fermion pairs, into the electroweak and strong interactions. Photon-photon interactions can be classified into three types of processes, illustrated in Fig. 13. Direct interactions involve only electroweak coupling, the once resolved process where one photon probes the parton structure of the other photon, similar to deep inelastic scattering, and the twice resolved process where the partons of each photon interact, similar to a $\rho - \rho$ collisions. We use the Pythia [36] Monte Carlo program to simulate the resolved photon cross sections which are potential backgrounds to *all* other two-photon physics processes. These backgrounds, usually referred to as $\gamma\gamma \to$ hadrons, are also a concern at e^+e^- and have been studied in detail [37]. However, at a $\gamma\gamma$ collider the high energy Compton photons provide an additional and dominant source of $\gamma\gamma \to$ hadron background. Nominally, we use the default settings for Pythia with the exception of the parameters listed in Table IV [38].

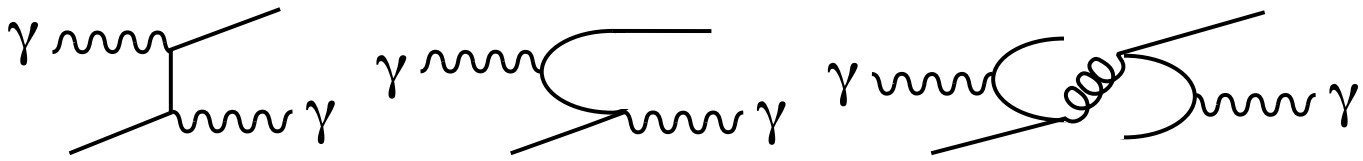

FIG. 13: Photon-photon Interactions. (left) Direct interactions involve only electroweak coupling. (center) Once resolved process where one photon probes the parton structure of the other photon, similar to deep inelastic scattering. (right) Twice resolved process where the partons of each photon interact, similar to a $\rho - \rho$ collisions.

Parameter Setting	Explanation
MSTP(14)=21	Direct gamma-gamma
MSTP(14)=24	Twice resolved photon
MSTP(14)=4	Once resolved photon
PARP(67)=4	fixes some problems with the initial
PARP(71)=4	and final state QCD radiation
CKIN(3)=1.0	ptmin for hard 2-¿2 interactions
PARP(81)=1.0	ptmin for final state interactions
MSTP(81)=1	Multiple interactions turned on (default)
MSTP(82)=1	Structure of multiple interactions (default)
PARP(90)=0.0	Removes energy scaling
PARP(89)=1.0	Rendered useless by papr(90)=0.0

TABLE IV: Pythia parameter settings for resolved photon processes.

We consider the beam parameters for $\sqrt{s}_{ee} = 150$ GeV and $\sqrt{s}_{ee} = 500$ GeV in Table I and use the luminosity distributions shown in Fig. 8. We process the events through the LC Fast MC detector simulation within ROOT [39], which includes calorimeter smearing and detector configuration as described in Section 4.1 of Chapter 15 of Ref. [40]. Our preliminary studies find that the two-photon cross section is dominated by the twice resolved process at both 150 GeV and 500 GeV. We find the once resolve event yield to be approximately 400 and 100 times larger than the direct cross section for 150 GeV and 500 GeV, respectively, and we find the twice resolve event yield to be approximately 1500 and 500 times larger than the direct cross section for 150 GeV and 500 GeV, respectively. However, these cross sections have large uncertainties which we discuss below. Most of the products of the $\gamma\gamma \to$ hadrons will be produced at small angles relative to the photon beam and will escape down the beam pipe undetected. We are interested in the decay products that enter the detector and we consider only tracks and showers with $|\cos\theta| < 0.9$ in the laboratory frame and we require tracks have to have momentum greater than 200 MeV and showers must have energy greater than 100 MeV. The resulting track and shower energy distributions integrated over 20,000 beam crossings for $\sqrt{s}_{ee} = 150$ GeV and 1,000 beam crossings for $\sqrt{s}_{ee} = 500$ GeV are shown in Fig. 15. Experimental, theoretical and modeling errors have not yet been evaluated for these distributions.

Future studies of the physics possibilities of a $\gamma\gamma$ collider should include the impact of resolved photons on the event reconstruction. The appropriate number of beam crossing to integrate over has not been determined. It is generally assumed that the $\gamma\gamma$ and e^+e^- detectors will be the same or at least have comparable performance. At e^+e^-, the plan is to integrate over 100's to 1000's of beam crossings. This depends, of course, on the choice of detector technology as well as the bunch structure of the electron beam. At a $\gamma\gamma$ collider experiment, the desire to minimize the resolved photon backgrounds may drive the detector design to integrate over as few beam crossings as possible. Thus the assumption that the e^+e^- and $\gamma\gamma$ detectors will be based on the same technology or have comparable performance may not be valid. An important distinction between the TESLA and NLC machine designs is the time between bunch crossings, 337 ns and 2.8 ns[4] , respectively. The authors plan to study the (hopefully) incremental difference between the design and performance of a detector for the $\gamma\gamma$ and e^+e^- interaction regions.

Large uncertainties plague the estimated once and twice resolved photon cross sections. Ref. [41] provides an ex-

[4] The NLC-e^+e^-design has 1.4 ns bunch spacing – see the caption of Table I for discussion.

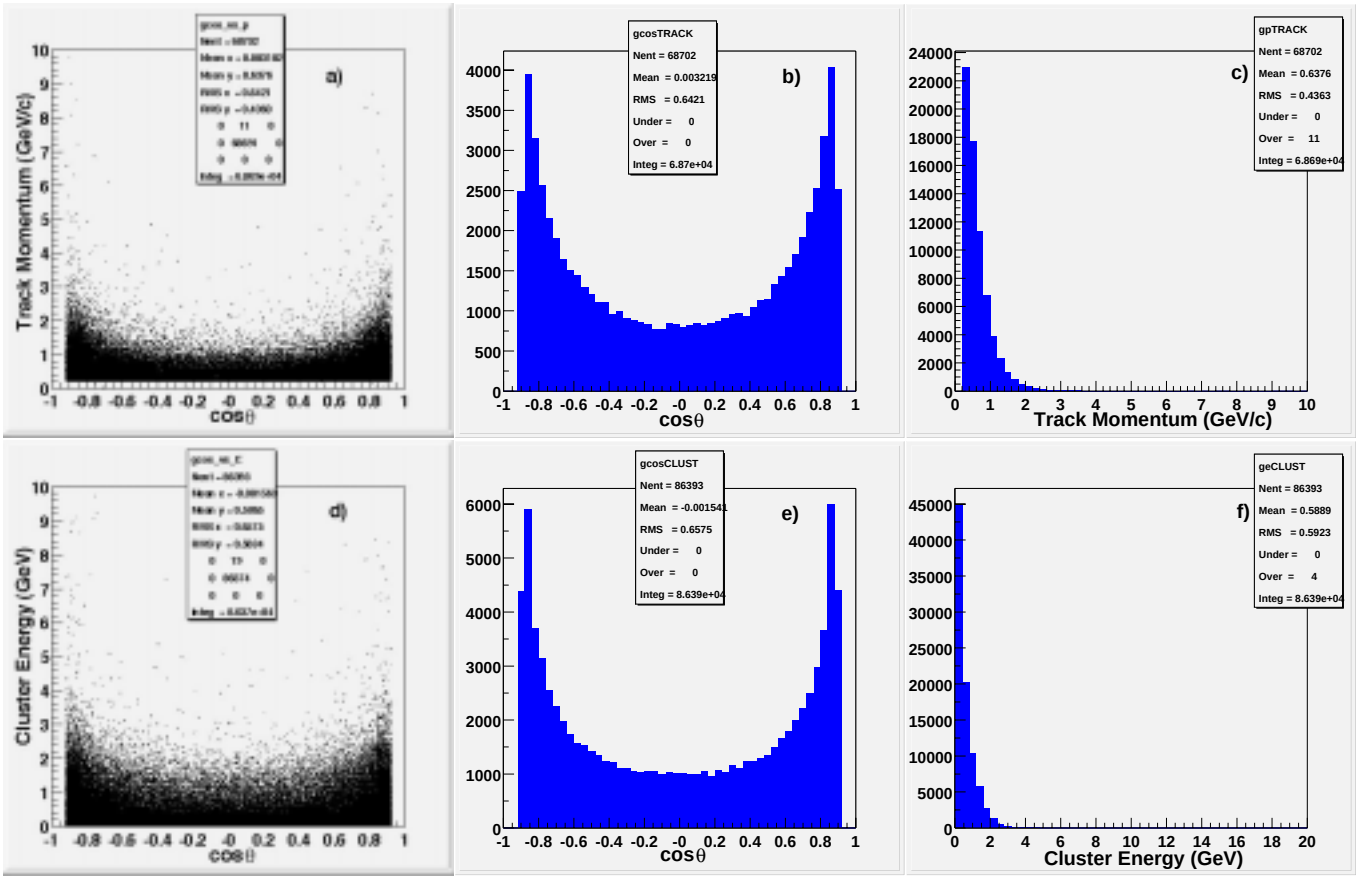

FIG. 14: Tracks and Shower contributing to the resolved photon background for $\sqrt{s}_{ee} = 150$ GeV a) Momentum versus $\cos\theta$ distribution for tracks with $p > 0.2$ GeV/c. b) and c) are the horizontal and vertical projections of a). d) Energy versus $\cos\theta$ distribution for showers with $E > 0.1$ GeV. e) and f) are the horizontal and vertical projections of d).

cellent discussion of the theoretical and experimental challenges of determining the photon structure. Most recent experimental data is from HERA [42] and LEP-II [43]. Large uncertaintes exist for small x_γ and significant uncertainties exist for large x_γ. The QCD stucture function is probed by examining high E_t jets. Extrapolating to smaller E_t introduces additional uncertainty. The situation may be improved by data obtained from a proposed $\gamma\gamma$ engineering run at SLC [44].

The impact of resolved photon backgrounds on the physics reach of a $\gamma\gamma$ collider has yet to be determined. Although unevaluated (and likely large) uncertainties in the expected track and shower momentum/energy distribution and normalization remain, we have incorporated the resolved photon background levels presented here into our analysis of $\gamma\gamma \to h \to \gamma\gamma$. The preliminary results are promising - see Section III.

IX. CONCLUSION

Several new results in the physics to be studied with $\gamma\gamma$ colliders have been briefly described. Most of these come from work in progress, and will be refined and extended over the next several months.

We believe that the next most important step is the study and understanding of resolved photon backgrounds, which appear to be formidable and possibly quite pernicious. They may force the detector design to differ significantly from the one currently under development for the e^+e^- linear collider. To this end, a proposal to perform a proof-of-principle experiment at SLAC is under way, and a workshop on the subject is planned for November, 2002.

In addition to understanding machine and background issues, it is time to take a closer look at the interplay of results expected from a high energy e^+e^- collider and a $\gamma\gamma$ collider. Discussions are already planned for LC2002, and should be continued at other workshops over the next year. A goal of such discussion should be a straw proposal for a combined run plan for, a 500 GeV machine with both e^+e^- and $\gamma\gamma$ interaction regions active.

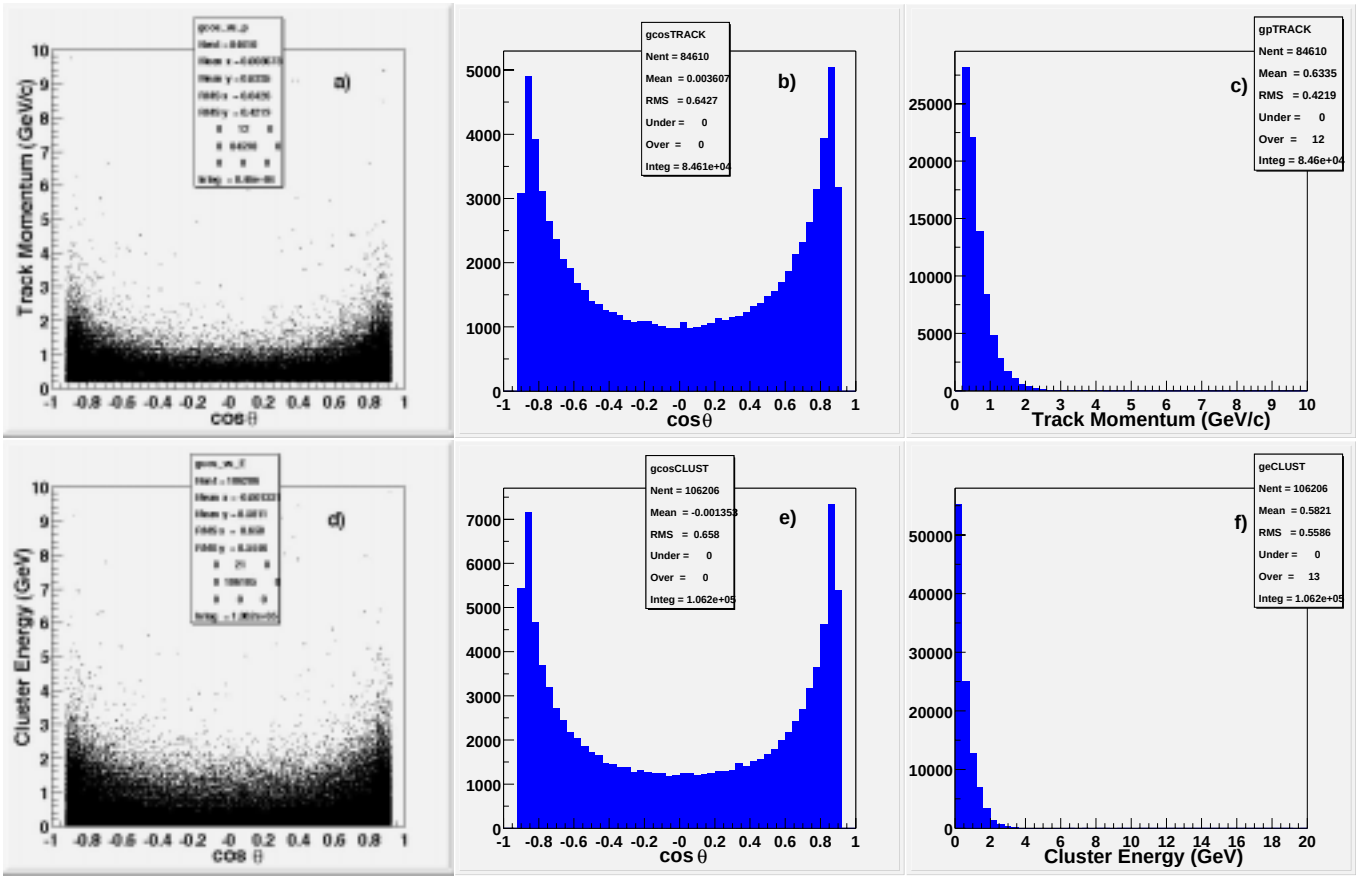

FIG. 15: Tracks and Shower contributing to the resolved photon background for $\sqrt{s}_{ee} = 500$ GeV a) Momentum versus $\cos\theta$ distribution for tracks with $p > 0.2$ GeV/c. b) and c) are the horizontal and vertical projections of a). d) Energy versus $\cos\theta$ distribution for showers with $E > 0.1$ GeV. e) and f) are the horizontal and vertical projections of d).

Acknowledgments

We are grateful to Jon Butterworth, Marcela Carena, Jeff Gronberg, Tony Hill, Steve Mrenna, and Michael Peskin for helpful discussions. Fermilab is operated by Universities Research Association Inc. under contract no. DE-AC02-76CH03000 with the U.S. Department of Energy. A portion of this work was performed under the auspices of the U.S. Department of Energy by the University of California, Lawrence Livermore National Laboratory under Contract No.W-7405-Eng.48. Other portions were supported by the Illinois Consortium for Accelerator Research, agreement number 228-1001. B.G. is supported in part by the State Committee for Scientific Research under grant 5 P03B 121 20 (Poland). J.F.G. is supported by the U.S. Department of Energy and by the Davis Institute for High Energy Physics.

[1] D. Asner *et al.*, arXiv:hep-ex/0111056;
[2] D. M. Asner, J. B. Gronberg and J. F. Gunion, arXiv:hep-ph/0110320.
[3] S. Soldner-Rembold and G. Jikia, Nucl. Instrum. Meth. A **472**, 133 (2001) [arXiv:hep-ex/0101056]; G. Jikia and S. Soldner-Rembold, Nucl. Phys. Proc. Suppl. **82**, 373 (2000) [arXiv:hep-ph/9910366].
[4] M. M. Velasco *et al.*, in *Proc. of the APS/DPF/DPB Summer Study on the Future of Particle Physics (Snowmass 2001)* ed. R. Davidson and C. Quigg, arXiv:hep-ex/0111055.
[5] J. A. Aguilar-Saavedra *et al.* [ECFA/DESY LC Physics Working Group Collaboration], "TESLA Technical Design Report Part III: Physics at an e^+e^- Linear Collider," arXiv:hep-ph/0106315; T. Abe *et al.* [American Linear Collider Working Group Collaboration], "Linear collider physics resource book for Snowmass 2001. 2: Higgs and supersymmetry studies," in *Proc. of the APS/DPF/DPB Summer Study on the Future of Particle Physics (Snowmass 2001)* ed. R. Davidson and C. Quigg, arXiv:hep-ex/0106056; K. Abe *et al.* [ACFA Linear Collider Working Group Collaboration], "Particle physics

experiments at JLC," arXiv:hep-ph/0109166.
[6] M. Battaglia and K. Desch, in *Physics and Experiments with Future Linear e^+e^- Colliders*, Proceedings of the 5th International Linear Collider Workshop, Batavia, Illinois, 2000, edited by A. Para and H. E. Fisk (AIP, Melville, NY, 2001), pp. 163-182 [arXiv:hep-ph/0101165].
[7] A. Djouadi, V. Driesen, W. Hollik and J. I. Illana, Eur. Phys. J. C **1**, 149 (1998) [arXiv:hep-ph/9612362].
[8] G. Belanger, F. Boudjema, T. Kon and V. Lafage, Eur. Phys. J. C **9**, 511 (1999) [arXiv:hep-ph/9811334].
[9] G. Belanger, F. Boudjema, T. Kon and V. Lafage, Eur. Phys. J. C **12**, 323 (2000) [arXiv:hep-ph/9907207].
[10] A. Djouadi, J. Kalinowski and M. Spira, Comput. Phys. Commun. **108**, 56 (1998) [arXiv:hep-ph/9704448].
[11] A. Djouadi, Phys. Lett. B **435**, 101 (1998) [arXiv:hep-ph/9806315].
[12] M. Carena, H. E. Haber, H. E. Logan and S. Mrenna, Phys. Rev. D **65**, 055005 (2002) [Erratum-ibid. D **65**, 099902 (2002)] [arXiv:hep-ph/0106116].
[13] S. Y. Choi, A. Djouadi, M. Guchait, J. Kalinowski, H. S. Song and P. M. Zerwas, Eur. Phys. J. C **14**, 535 (2000) [arXiv:hep-ph/0002033].
[14] S. Y. Choi, J. Kalinowski, G. Moortgat-Pick and P. M. Zerwas, Eur. Phys. J. C **22**, 563 (2001) [Addendum-ibid. C **23**, 769 (2002)] [arXiv:hep-ph/0108117].
[15] A. Djouadi, V. Driesen, W. Hollik and A. Kraft, Eur. Phys. J. C **1**, 163 (1998) [arXiv:hep-ph/9701342].
[16] D. Dominici, B. Grzadkowski, J. F. Gunion and M. Toharia, arXiv:hep-ph/0206192.
[17] T. Abe *et al.* [American Linear Collider Working Group Collaboration], in *Proc. of the APS/DPF/DPB Summer Study on the Future of Particle Physics (Snowmass 2001)* ed. R. Davidson and C. Quigg, arXiv:hep-ex/0106056. See sections 8.5 and 8.6, and Table 3.2.
[18] M. A. Diaz, S. F. King and D. A. Ross, Nucl. Phys. B **529**, 23 (1998) [arXiv:hep-ph/9711307]; T. Blank and W. Hollik, arXiv:hep-ph/0011092.
[19] T. Mayer and H. Fraas, Nucl. Instrum. Meth. A **472**, 165 (2001) [arXiv:hep-ph/0009048]; C. Blochinger, H. Fraas, T. Mayer and G. Moortgat-Pick, in *Physics and Experiments with Future Linear e^+e^- Colliders*, Proceedings of the 5th International Linear Collider Workshop, Batavia, Illinois, 2000, edited by A. Para and H. E. Fisk (AIP, Melville, NY, 2001), pp. 447-451 [arXiv:hep-ph/0101176].
[20] M. L. Zhou, W. G. Ma, L. Han, Y. Jiang and H. Zhou, J. Phys. G **25**, 1641 (1999) [arXiv:hep-ph/9903376].
[21] H. Eberl, M. Kincel, W. Majerotto and Y. Yamada, Phys. Rev. D **64**, 115013 (2001) [arXiv:hep-ph/0104109].
[22] M. Koike, T. Nonaka and T. Kon, Phys. Lett. B **357**, 232 (1995) [arXiv:hep-ph/9504309].
[23] P. Raimondi and A. Seryi, Phys. Rev. Lett. **86**, 3779 (2001).
[24] D. Asner, talk presented to SLAC LCD Meeting, January 15, 2002.
http://www-sldnt.slac.stanford.edu/nld/meetings/2002/20020115/slac_lc.pdf.
[25] D. Asner *et al.*, PAC-2001-FPAH055 *Presented at IEEE Particle Accelerator Conference (PAC2001), Chicago, Illinois, 18-22 Jun 2001.*
[26] P. Chen *et al.*, Nucl. Instrum. Meth. **A355**, 107 (1995).
http://www-acc-theory.kek.jp/members/cain/cain21b.manual/main.html.
[27] I. F. Ginzburg *et al.*, Nucl. Instrum. Meth. **205**, 47 (1983).
[28] I. F. Ginzburg *et al.*, Nucl. Instrum. Meth. A **219**, 5 (1984).
[29] D. J. Miller and S. Moretti, Eur. Phys. J. C **13**, 459 (2000) [arXiv:hep-ph/9906395]; A. Djouadi, W. Kilian, M. Muhlleitner and P. M. Zerwas, Eur. Phys. J. C **10**, 27 (1999) [arXiv:hep-ph/9903229].
[30] C. Castanier, P. Gay, P. Lutz and J. Orloff, arXiv:hep-ex/0101028.
[31] U. Baur, T. Plehn and D. Rainwater, arXiv:hep-ph/0206024; F. Gianotti *et al.*, arXiv:hep-ph/0204087.
[32] G. V. Jikia, Nucl. Phys. B **412**, 57 (1994).
[33] T. Hahn and M. Perez-Victoria, Comput. Phys. Commun. **118**, 153 (1999) [arXiv:hep-ph/9807565]; see `www.feynarts.de`.
[34] The results of Fig. 9 were provided by F. Gianotti on behalf of the ATLAS collaboration. They are the preliminary results available as of March 3, 2001.
[35] M. Iwasaki and M. Peskin.
http://www-sldnt.slac.stanford.edu/nld/new/Docs/Generators/PANDORA.htm
http://www-sldnt.slac.stanford.edu/nld/new/Docs/Generators/PANDORA_PYTHIA.htm
[36] T. Sjostrand, hep-ph/9508391. T. Sjostrand, P. Eden, C. Friberg, L. Lonnblad, G. Miu, S. Mrenna and E. Norrbin, hep-ph/0010017. See the PYTHIA and JETSET web pages, http://www.thep.lu.se/~torbjorn/Pythia.html.
[37] D. Schulte, TESLA 97-08, 1996, http://tesla.desy.de/TTF_Report/TESLA/TTFnot97.html;
C. Hensel, LC-DET-2000-001, 2000, http://www.desy.de/~lcnotes/.
[38] Jon Butterworth – Private Communication.
[39] R. Brun and F. Rademakers, Nucl. Instrum. Meth. A **389**, 81 (1997).
[40] T. Abe *et al.* [American Linear Collider Working Group Collaboration], hep-ex/0106058.
[41] J. M. Butterworth, in *Proc. of the 19th Intl. Symp. on Photon and Lepton Interactions at High Energy LP99* ed. J.A. Jaros and M.E. Peskin, Int. J. Mod. Phys. A **15S1**, 538 (2000) [eConf **C990809**, 538 (2000)] [arXiv:hep-ex/9912030].
[42] B. Andrieu [H1 and ZEUS Collaborations], J. Phys. G **28**, 823 (2002).
[43] A. Csilling, arXiv:hep-ex/0112020.
[44] We plan to demonstrate the technical feasibility of the NLC $\gamma\gamma$ interaction region design. We propose to integrate a 1/2 scale NLC $\gamma\gamma$ interaction region into the SLC and generate two-photon luminosity by Compton scattering 30 GeV beams from the SLC off a 0.1 J short pulse laser.